NANO · MICRO small
www.small-journal.com

Bi-Functional Electrolyte Additive Leading to a Highly Reversible and Stable Zinc Anode

Mingcong Tang, Qun Liu, Zhenlu Yu, Xiaohong Zou, Xiaoyu Huo, Biao Zhang, and Liang An**

A stable stripping/plating process of the zinc anode is extremely critical for the practical application of aqueous zinc metal batteries. However, obstacles, including parasitic reactions and dendrite growth, notoriously deteriorate the stability and reversibility of zinc anode. Herein, Methyl l-α-aspartyl-l-phenyl-alaninate (Aspartame) is proposed as an effective additive in the $ZnSO_4$ system to realize high stability and reversibility. Aspartame molecule with rich polar functional groups successfully participates in the solvation sheath of Zn^{2+} to suppress water-induced side reactions. The self-driven adsorption of Aspartame on zinc anode improves uniform deposition with a dose of 10 mM. These synergetic functions endow the zinc anode with a significantly long cycling lifespan of 4500 h. The cell coupled with a vanadium-based cathode also exhibited a high-capacity retention of 71.8% after 1000 cycles, outperforming the additive-free counterparts.

1. Introduction

Rechargeable aqueous zinc metal batteries (AZMBs) have emerged as a promising energy storage and conversion technique owing to their acceptable redox potential (−0.76 V vs standard hydrogen electrode), high theoretical capacity (820 mAh g^{-1}, or 5855 mAh cm^{-3}),[1] and inherent safety.[2] Unfortunately, unfavorable anodic interfacial reactions and zinc dendrite growth hinder the commercialization of AZMBs. Specifically, the mild acid nature and narrow electrochemical stability window cause the continuous hydrogen evolution reaction, resulting in the local enrichment of OH^-.[3] Accompanied by-product generation will induce surface passivation. Meanwhile, the aggregation of Zn^{2+} during deposition happened due to the strong local electrical field caused by tips, resulting in rampant dendrite growth causing the issue of internal short circuits.

To facilitate the reliable operation of AZMBs, numerous intriguing strategies have been proposed to address the above issues. Improvement of anode stability can be achieved through two approaches: modification of the electrode surface via morphology development[4] or protective layer,[5] and optimization of electrolyte solvent shell.[6] Modifications in Zn anode morphology can be accomplished by fabricating 3D structures or eliminating inherent strain. Meanwhile, the zinc surface can be coated with an effective layer. For example, functional materials such as metals, metal oxides,[7] polymers,[5b,8] and carbon materials[9] have been extensively investigated as protective layers. However, these strategies are hard to implement due to their complex procedures.

Electrolyte engineering that can be easily handled appears to be more promising for translating scientific advancements into actual practice. Therefore, a broad range of electrolyte additives have been investigated. Some additives like organic solvents or salts with high solubility are used to form co-solvent electrolytes[10] or "water in salts" electrolytes,[11] respectively. However, organic solvents and concentrated salts lead to high viscosity impeding the ion transport. Additionally, flammable solvents are also harmful to the inherent safety of aqueous electrolytes. Therefore, the limited addition of appropriate additives into the aqueous electrolyte is more convenient and safer. Currently, numerous additives have been reported. Additives including polyethylene glycol-400,[12] 2-Bis(2-hydroxyethyl) amino-2-(hydroxymethyl)-1,3-propanediol,[13] Tridentate citrate,[14] Glucose,[15] and Cyclodextrins[16] are reported effective for inhibiting water-induced parasitic reactions by replacing water molecules within solvation sheath. Other additives like polyethylene glycol-8000,[17] polyethyleneimine-800,[18]

M. Tang, X. Zou, X. Huo, L. An
Department of Mechanical Engineering
The Hong Kong Polytechnic University
Hung Hom, Hong Kong 999077, China
E-mail: liang.an@polyu.edu.hk

Q. Liu, Z. Yu, B. Zhang
Department of Applied Physics
The Hong Kong Polytechnic University
Hung Hom, Hong Kong 999077, China
E-mail: biao.ap.zhang@polyu.edu.hk

L. An
Research Institute for Advanced Manufacturing
The Hong Kong Polytechnic University
Hung Hong, Kowloon, Hong Kong SAR 999077, China

The ORCID identification number(s) for the author(s) of this article can be found under https://doi.org/10.1002/smll.202403457

DOI: 10.1002/smll.202403457

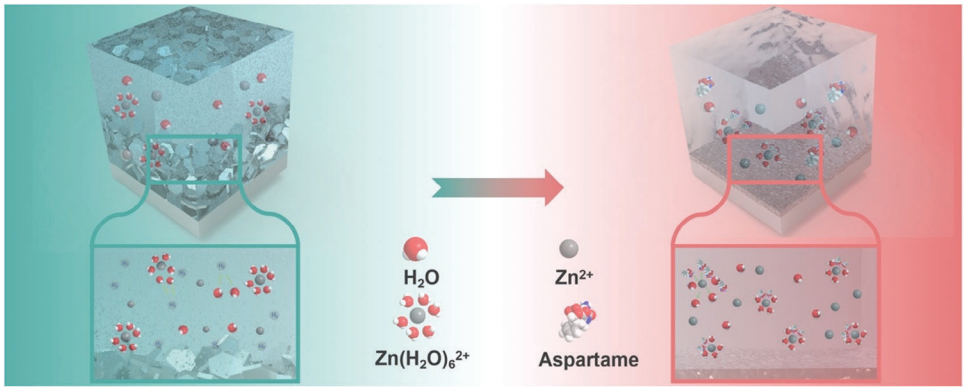

Scheme 1. Schematic illustration of Aspartame influence for Zn anode in ZSO electrolyte system.

ethylene diamine tetraacetic acid tetrasodium,[19] and tetrabutylammonium sulfate[20] help establish an adhesive layer on zinc surface. Their rich polar functional groups exert attractive force to derive uniform deposition of Zn^{2+}. Furthermore, some additives (Urea[21] and Succinonitrile)[22] can be incorporated with zinc salts to form eutectic electrolytes. Nevertheless, there remain issues with these proposed additives: 1) Favorable dosages for several additives are excessive (0.1 M, or even up to 70 wt%),[23] increasing the material cost and viscosity. 2) Additives insoluble in water entail organic zinc salts like $Zn(TFSI)_2$ and $Zn(OTF)_2$ to improve the solubility. These organic zinc salts are expensive and possess a high molar weight, so issues like high cost and low energy density[24] happen; 3) Insufficient polarity may cause weak surface adhesion, so additives will be continuously consumed. As a result, the protection is inconsistent, and the final advancement of stability is not remarkable. Such a consideration inspires the usage of a trace amount of additive with multifunction to address these problems.

In this work, we reported Methyl l-α-aspartyl-l-phenylalaninate (Aspartame) with luxuriant O, N—contained polar functional groups (C═O, -NH_2 and O═C—OH) (Figure S1, Supporting Information) as an ultra-stable additive in conventional 2.0 M $ZnSO_4$ electrolyte to realize extremely reversible zinc anode with trace amount (0.186 wt%). It revealed functions for suppressing parasitic reactions by regulating the solvent structure of Zn^{2+}, and deriving a more uniform deposition process through adsorption on zinc surface as demonstrated in **Scheme 1**. Combining these double functions of Aspartame, 10 mM Aspartame functions the best to extend the lifespan of Zn||Zn symmetric cells up to 4500 h under 2 mA cm^{-2}, which is among the overwhelming in recent published additives. More astonishingly, a three-times improvement in symmetric cells duration is achieved using only 1 mM Aspartame. Moreover, ultra-high Coulombic Efficiency (99.78% at 8 mA cm^{-2}), and long stable operation (300 h) with limited zinc supply (70% Depth of discharge) presented astonishing reversibility. Besides, the improvement in reversibility and stability also applies to Zn||$Cu_xV_2O_5$ full cells. As expected, the fabricated Zn||$Cu_xV_2O_5$ full batteries obtain a capacity retention of 71.8% after 1000 cycles under a high specific current density of 10 A g^{-1}. All these improvements indicate the efficacy of Aspartame for stabilizing zinc anode to reach extremely effective AZMBs.

2. Results and Discussion

The solvation interaction between Aspartame and $ZnSO_4$, and the mechanism of surface adsorption were first confirmed through both theoretical calculations and multiple techniques of spectroscopy. Binding energies between Zn^{2+} and three oxygen-containing functional groups (O═C—OH, O═C—OCH_3, and O═C—NH) have been evaluated through the density functional theory (DFT) calculation (**Figure** 1b; Figure S2, Supporting Information). The binding energy between Zn^{2+} and these three functional groups can reach −20.82, −16.36, and −24.59 kcal mol^{-1} respectively. Among all three functional groups, O═C—NH shows a much more robust binding energy (−24.59 kcal mol^{-1}) compared with that between Zn^{2+} and water molecules (−19.45 kcal mol^{-1}). This increased binding energy indicates an inclination for Aspartame to participate in the solvation sheath of Zn ions.[25] As depicted in the electrostatic potential mapping (Figure 1a), C═O and —COOH groups of Aspartame, and O atom of H_2O show more negative charge distribution. Moreover, once one water molecule is replaced by one Aspartame molecule, the electrostatic mapping shows more inhomogeneous ascribed to C═O and —COOH groups, which effectively alleviates electrostatic attraction around Zn^{2+}, and therefore fastens transportation of Zn^{2+}. As depicted in Figure S3 (Supporting Information), the Zn^{2+} transference number also confirms the boosting cation transportation. With the addition of 10 mM Aspartame, the Zn^{2+} transference number (t_{Zn}^{2+}) exhibits a high value of 0.556, superior to t_{Zn}^{2+} of 2.0 M $ZnSO_4$ electrolyte (0.452). For further verifying the roles of Aspartame in solvation sheath, Raman spectroscopic measurement and Fourier transform infrared spectroscopy (FTIR) were conducted. In Figure 1c, one peak can be observed at ≈3414 cm^{-1}, which is the typical location of the O—H stretching vibration, and with increasing concentration, a blue shift can be observed and the O—H stretching vibration is successfully suppressed. This modification of H-bonds can also be confirmed through a shift to a lower wavenumber of transmittance in FTIR results (Figure 1e). This indicates the break of original H-bonds and the increasing proportion of strong H-bonds. A higher proportion of strong H-bonds contributes to weaker water activity and suppression of water-induced parasitic reactions.[26] The Raman spectra were also conducted on a wavenumber between 900–1100 cm^{-2}, representing $\nu(SO_4^{2-})$, to identify the solvation structure more clearly.

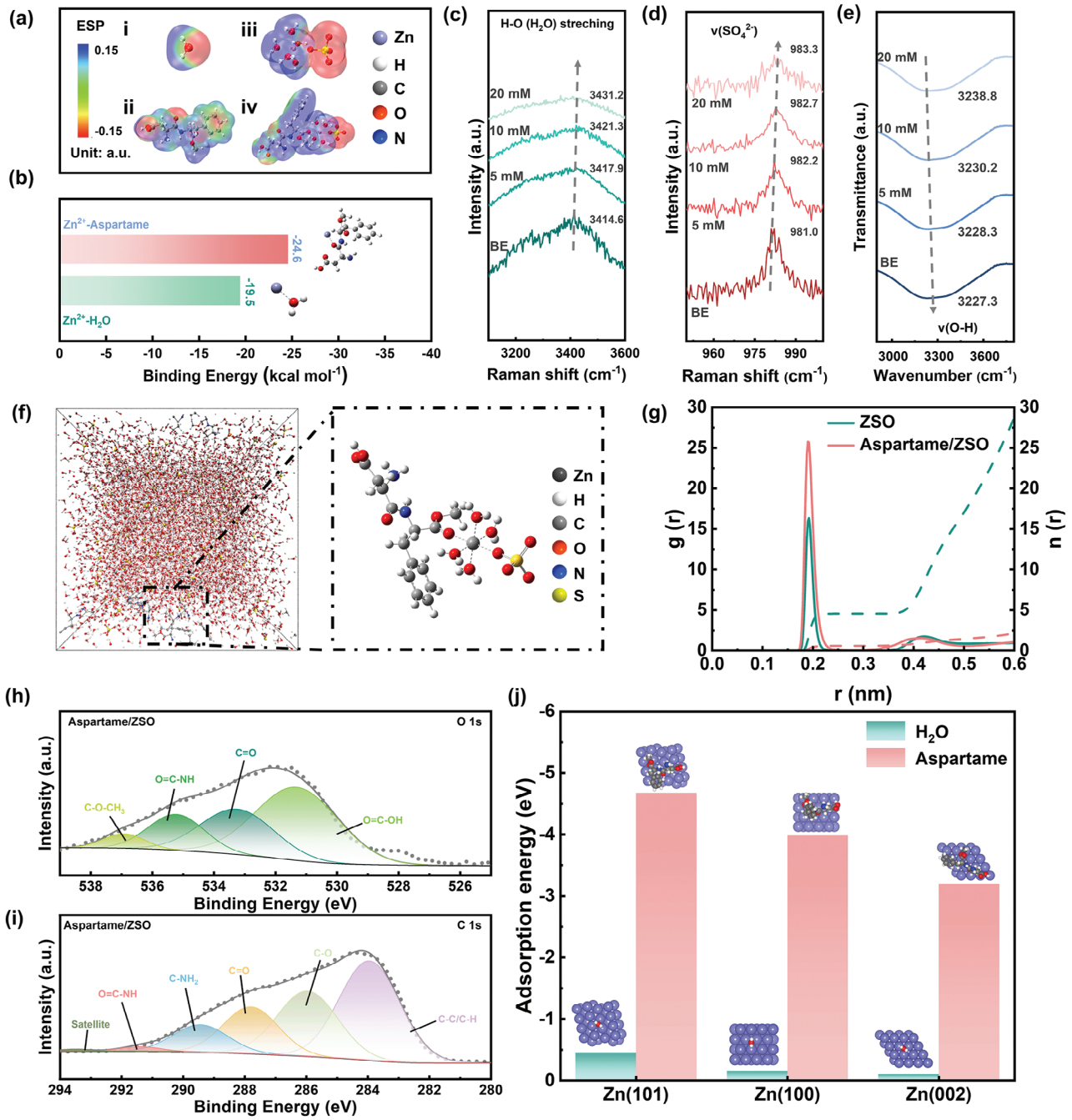

Figure 1. a) Electrostatic mapping of (i). water molecule, (ii). Aspartame molecule, (iii). pristine Zn^{2+} – $5H_2O$-SO_4^{2-} solvation structure and (iv). Aspartame-Zn^{2+} – $4H_2O$-SO_4^{2-}. (b) Binding energy between Zn^{2+}-H_2O, and Zn^{2+}-Aspartame. c,d) Raman spectra of 2 M $ZnSO_4$ electrolytes with different concentrations of Aspartame. e) FTIR spectra of 2 M $ZnSO_4$ electrolytes with different concentrations of Aspartame. f) Snapshot of electrolyte obtained from MD simulations and partially enlarged snapshot expressing Zn^{2+} solvation structure. g) The radial distribution function (RDF) results of various electrolytes. The high-resolution XPS spectra of Zn surface after Aspartame adsorption: h) O 1s, i) C 1s. j) Adsorption energies of H_2O and Aspartame molecules on Zn (101), Zn (100), and Zn (002) planes.

The traditional Eigen–Tamm (ET) mechanism divided ion-pairs species into two major clusters: solvation-separated ion pair (SSIP, $[Zn^{2+}\text{-}(H_2O)_n{\cdot}SO_4^{2-}]$), and contact ion pair (CIP, $[Zn^{2+}\text{-}(H_2O)_{n-1}{\cdot}OSO_3^{2-}]$).[27] As demonstrated in Figure 1d, Aspartame content resulted in a shift to higher frequency with increasing concentration, demonstrating a lower CIP proportion. Thus, it is more difficult for SO_4^{2-} species to participate in the inner solvation sheath, substantiating efficient regulation of Zn^{2+} surrounding environment brought by Aspartame. Molecular dynamics (MD)simulations are carried out to reveal the solvation structure of Zn^{2+} in the 2.0 M $ZnSO_4$ (ZSO) and in 2.0 M $ZnSO_4$ with 10 mM Aspartame (Aspartame/ZSO) systems (Figure 1f,g;

Figure S4, Supporting Information). As presented by snapshots, one water molecule can be replaced by one Aspartame molecule, suggesting optimization of the solvation sheath. After conducting the radius distribution functions (RDF) for analyzing the average coordination number (ACN), for pristine ZSO electrolyte, a peak of Zn-O at ≈0.19 nm to the core of Zn^{2+} should be attributed to H_2O molecules in the solvation sheath with the coordination number of 4.56. Similarly, with the addition of Aspartame, the peak of Zn-O attributed to Aspartame is also at ≈0.19 nm with the coordination number of 0.60, suggesting the occupation of Aspartame on solvation sheath.

Surface adsorption was first confirmed through X-ray photoelectron spectroscopy (XPS). From previous studies, electron-rich carbonyl groups obtained a tendency to donate electrons.[26] This characteristic endows Aspartame with self-driven adsorption behavior.[28] The adsorption of Aspartame on the zinc surface was confirmed through X-ray Photoemission Spectroscopy (XPS). Considering that functional groups on Aspartame molecules are mostly O-contained groups, C 1s, and O 1s spectra were tested. First, XPS results of pure Aspartame powder were presented in Figure S5a,b for comparison. As shown in Figure S5a, peaks of O—C—CH_3, O═C-NH, C═O, and O═C—OH can be found, while peaks of C—C, C—O, C═O, C—NH_2, O═C—NH, and its satellite peak can be observed in Figure S5b. The same spectrum was tested for surfaces of zinc foils immersed in Aspartame/ZSO electrolyte for 24 h and washed with deionized water. As indicated in Figure 1h,i, the same bonding found in Aspartame powder was also identified on the O 1s and C 1s spectrum on treated zinc foil. This self-driven adsorption can be ascribed to the formation of electron donors (carbonyl functional groups) and electron acceptor (zinc foil surface) pairs. These carbonyl functional groups could play the role of pincer-like adsorption anchors.[28]

Moreover, the DFT calculations indicated that the adsorption energies of the Aspartame molecule on three zinc crystal planes (101), (100), and (002) are −4.67, −3.99, and −3.19 eV correspondingly. On the contrary, the adsorption energies of H_2O on these planes are only −0.45, −0.15, and −0.11 eV, respectively (Figure 1j). This elevation of adsorption energies suggests a strong interaction between zinc metal anode and Aspartame molecules, deriving a tendency for surface adsorption of Aspartame.

With limited water content in the solvation structure, H_2O-induced side reactions should be suppressed. Linear sweep voltammetry (LSV) test was carried out to analyze the capability of Aspartame on corrosion resistance. Tafel line was obtained through LSV result treated with extrapolation (**Figure 2**a), showing much lower corrosion current (19.21 mA cm^{-2}) for Zn anode in Aspartame/ZSO electrolyte, superior to that of ZSO electrolyte (185.57 mA cm^{-2}). This slower corrosion rate indicates functional relief of self-corrosion issues with the Aspartame additive. LSV measurements were also conducted to study hydrogen and oxygen evolution behavior during the plating and stripping process. As shown in Figure 2b,c, oxygen evolution reaction (OER) potential is increased from 2.53 to 2.57 V, and hydrogen evolution reaction (HER) potential is decreased from −0.133 to −0.177 V by replacing ZSO with Aspartame/ZSO electrolyte, manifesting suppression of both HER and OER. This alleviation of both chemical and electrochemical corrosion was verified through contact angle measurement, X-ray Diffraction (XRD) spectroscopy, and integrated visualization evaluation. Contact angles between different electrolytes and zinc foils were measured with both pristine zinc plate and zinc treated by being soaked for 24 h. Specifically, the contact angle between ZSO and pristine zinc, and between Aspartame/ZSO and pristine zinc did not show obvious trends for forming a zincophilic interface (Figure 2d,e). However, the contact angle between the ZSO electrolyte and the zinc surface showed a sharp decrease from 90.53° to 27.31° once the zinc foil was immersed and corroded for 24 h. On the contrary, Aspartame/ZSO electrolyte shows similar contact angles of 90.41° and 80.29° on pristine and treated zinc foil respectively (Figure 2e). Moreover, this trend became even more obvious with a longer time of treatment (Figure S6, Supporting Information). The dramatic reduction in contact angle between zinc and ZSO electrolyte indicated the improved hydrophilicity brought by widely presented byproducts (zinc oxide, zinc hydroxide, etc.), which are intrinsically hydrophilic due to rich hydroxyl groups. Therefore, a slight decline of contact angle with Aspartame/ZSO electrolyte shows limited by-products. Precise amounts of byproducts were excavated through XRD spectroscopy of both deposited and soaked zinc plates. As shown in Figure 2f, the XRD pattern of zinc foil detached from Zn||Zn cells operated under 8 mA cm^{-2} for 10 cycles showed peaks of $Zn_4(OH)_6SO_4{\cdot}5H_2O$ for zinc foil cycled with ZSO electrolyte, and no peaks of byproducts appear on samples with Aspartame/ZSO electrolyte. A similar contrasting condition is observed on XRD patterns for soaked zinc. Peaks of $Zn_4(OH)_6SO_4{\cdot}5H_2O$ emerged on zinc immersed in ZSO for 24 h and became extremely intensive once treatment lasted for 100 h (Figure 2g). The intensive generation of byproducts can also be observed on the surface of zinc immersed in the ZSO electrolyte (Figure 2h; Figure S7, Supporting Information). A non-uniform layer can be observed through both digital and microscopic pictures and layered byproducts with a size larger than 20 µm can be found. Contrarily, the surface of samples treated with Aspartame/ZSO remained similar to pristine zinc plate without any by-products (Figure 2i; Figure S8, Supporting Information).

Apart from parasitic reactions, deposition behavior can be tailored because of the surface adsorption of Aspartame. As evidence, a series of optical and electrochemical measurements were carried out for excavate deposition mode in detail. First, the nucleation behavior along with deposited surface morphology was verified through the Chronoamperometry (CA) test by recording current response under a constant voltage of −0.15 V. As shown in **Figure 3**a, fast decreasing trend of current is presented with ZSO electrolyte in Zn||Zn symmetric cell, and stability cannot be achieved within 300 s. The unstable current signal indicates a 2D diffusion mode of deposition and an increasingly more severe "tip effect" resulting in unstoppably magnified surface areas. Oppositely, participation of Aspartame prompts a stable current within 50 s (Figure 3b), and a steady state is reached more quickly with a higher concentration of Aspartame (Figure S9, Supporting Information). This indicates a denser deposition layer with a finer nucleus caused by 3D deposition. The primary nucleation process generating smaller and more uniform nuclei aimed by Aspartame can be substantiated through the increase of nucleation overpotential from 108.1 to 134.7 mV under a current density equal to 8 mA cm^{-2} (Figure 3c). Typically, there is a

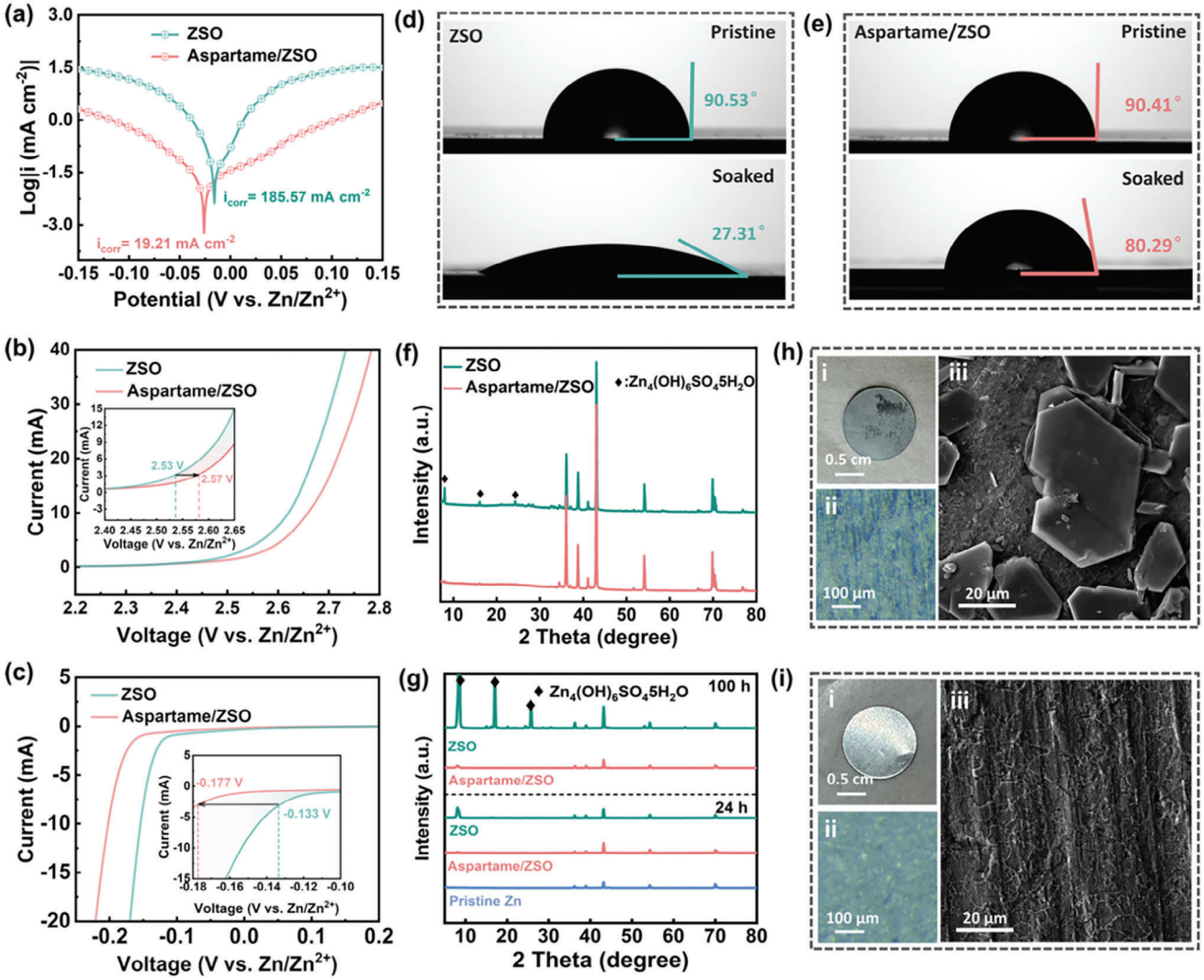

Figure 2. a) Linear polarization curves of Zn plate tested in ZSO and Aspartame/ZSO electrolytes with a scan rate of 5 mV s^{-1}. b) OER and c) HER tests using LSV measurement tested by the Zn||SS asymmetric cells in different electrolytes with the scan rate of 5 mV s^{-1}. d) Contact angle of ZSO electrolyte on Zn before and after soaking for 24 h in ZSO electrolyte. e) Contact angle of Aspartame/ZSO electrolyte on Zn before and after soaking for 24 h in Aspartame/ZSO electrolyte. XRD patterns of the Zn plate f) operated for 10 cycles under 8 mA cm^{-2}, and g) immersed in ZSO and Aspartame/ZSO for 24 h and 100 h. h) (i). Digital picture, (ii). Microscopic images, and (iii). SEM images of the Zn anode surface after being immersed in the ZSO electrolyte. (i) i. Digital picture, (ii). Microscopic images, and iii. SEM images of the Zn anode surface after being immersed in Aspartame/ZSO electrolytes.

critical value of the radius of the nucleus can be obtained through Equation (1).[29]

$$r_c = Ah\sigma / (\rho nF\eta) \quad (1)$$

In Equation (1), A is the atomic mass, and h is the height of the Zn atom. σ is the tension on the interface between electrode and electrolyte, ρ is the density of the nucleus, n is the valence of zinc ions, F is Faraday's constant, and η is the overpotential. Because the radius of nuclei needs to be larger than r_c to exist and grow, smaller critical radium would result in a diminutive and uniform nucleus. Therefore, a higher nucleation overpotential means a more efficient nucleation driving force, evoking a preference for fine-grained nuclei to avoid the generation of protrusions. For uncovering actual nucleation and deposition behavior, in situ optical observation was conducted by continuously depositing 10 mAh Zn. As shown in Figure 3d, with ZSO electrolyte, ≈15 μm zinc was accumulated within 1 h, and sporadic spots emerged at the beginning 10 m to form tips. With prolonged deposition time, these tips started to aggregate forming protrusions, and defects became even more obvious, resulting in high risks of dendrites-induced short-circuits. Adversely, surface evolution is extremely distinctive for the deposited layer with Aspartame/ZSO electrolyte. With Aspartame, the thickness of the deposited layer is also ≈15 μm, and the nucleus is much smaller from the beginning of deposition with no protuberances for the whole deposition process (Figure 3e). Furthermore, scanning electron microscope (SEM) images were taken for zinc anodes after different cycles. Figure 3f–h exhibits SEM images of zinc anodes after operating with ZSO electrolyte for 1 cycle, 30

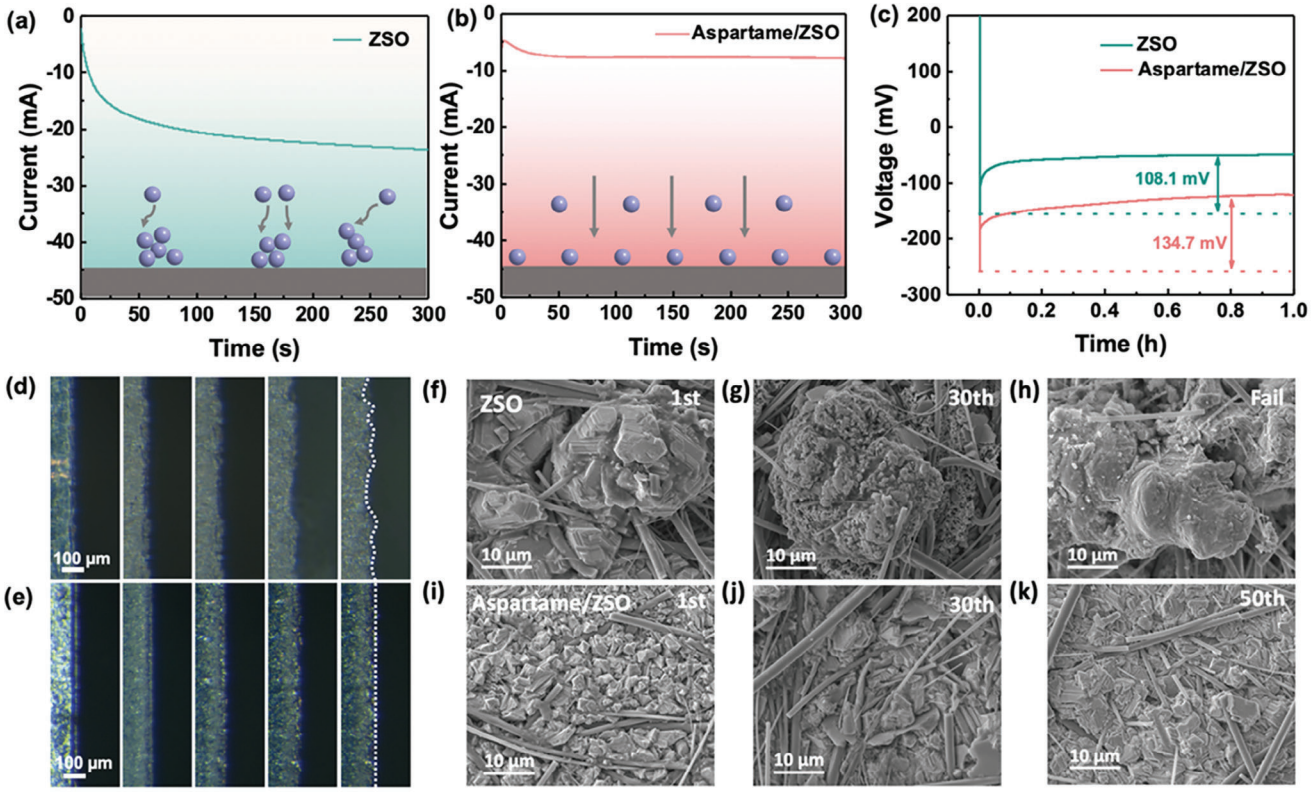

Figure 3. The current-time profiles of the Zn||Zn symmetric cells with a) ZSO electrolyte, and b) Aspartame/ZSO electrolyte with inset showing the schematic demonstration of Zn^{2+} diffusion. c) The initial Zn nucleation overpotentials using Zn||Cu half cells at 8 mA cm^{-2} in different electrolytes. In situ optical microscope observation of Zn deposition in d) ZSO electrolyte, and e) Aspartame/ZSO electrolyte for 1 h with a current density of 10 mA cm^{-2}. SEM images of Zn anodes after f) 1 cycle, g) 30 cycles, and h) cycled until failure in ZSO electrolyte. SEM images of Zn anodes after i) 1 cycle, j) 30 cycles, and k) 50 cycles in Aspartame/ZSO electrolyte.

cycles, and cycling to a short circuit. Aggregated zinc emerged at the very beginning cycle to form an uneven nucleus with a radius larger than 25 μm, resulting in rough morphology posing sharp edges. This aggregated zinc tends to grow with prolonged operation, which indicates fast and uncontrollable accumulation of byproducts and dendrites. In sharp contrast, the nucleus found on zinc anodes after the same time of cycling with Aspartame/ZSO electrolyte obtained a much smaller size to form a denser and planer surface from 1 cycle to 50 cycles, as shown in Figure 3i–k, effectively relieving the risk of separator penetration.

Combining these multiple merits including parasitic reactions resistance and derivation of uniform deposition, the reversibility and stability of zinc anode should be improved to a promising extent. For catching veritable improvement in zinc anode, symmetric cells were fabricated and evaluated under different current densities. First, the optimal concentration of Aspartame in practicable cells was determined depending on the lifespan of symmetric cells (Figure S10, Supporting Information), because both ionic conductivity and pH values do not show obvious favorable or unfavorable trends with varying Aspartame (Figures S11 and S12, Supporting Information). Lifespan shows a linearly increasing trend when the concentration varied from 1.0 to 10 mM, and even a trace amount of additive (1.0 mM) could provide a three-times extension of lifespan (Figure S13, Supporting Information). Once the concentration was increased to 20 mM, the stability degraded suddenly. The relatively unfavorable performance of 20 mM Aspartame can be ascribed to difficult deposition due to the high energy barrier during the de-solvation process (Figure S14, Supporting Information). The result is consistent with increasing charge transfer resistance indicated by EIS tests (Figure S15, Supporting Information). Therefore, 10.0 mM Aspartame was chosen as the most optimal design for investigations as Aspartame/ZSO. With ZSO electrolyte, unstable plating/stripping voltage happened at 87th cycles, and a short circuit immediately happened in the following 88th cycle under a current density of 2 mA cm^{-2}. This indicates poor reversibility of zinc anodes, severe issues of dendrite growth, and drastic parasitic reactions. Contrarily, Zn||Zn cells with Aspartame/ZSO reached a lifespan of up to 4500 h under the same current density and capacity without significant fluctuation of voltage signals, presenting an extremely high accumulated areal capacity of 9 Ah cm^{-2} which is among the overwhelming compared with most published electrolyte engineering strategies (**Figure** 4f; Table S1, Supporting Information). Rate performance tests and stability measurements with other current densities were also conducted to confirm that this improvement can be applied to a broad range of working conditions. As indicated in Figure 4b, current densities increased from 0.5 to 20 mA cm^{-2} for 5 cycles and then returned to 2 mA cm^{-2}.

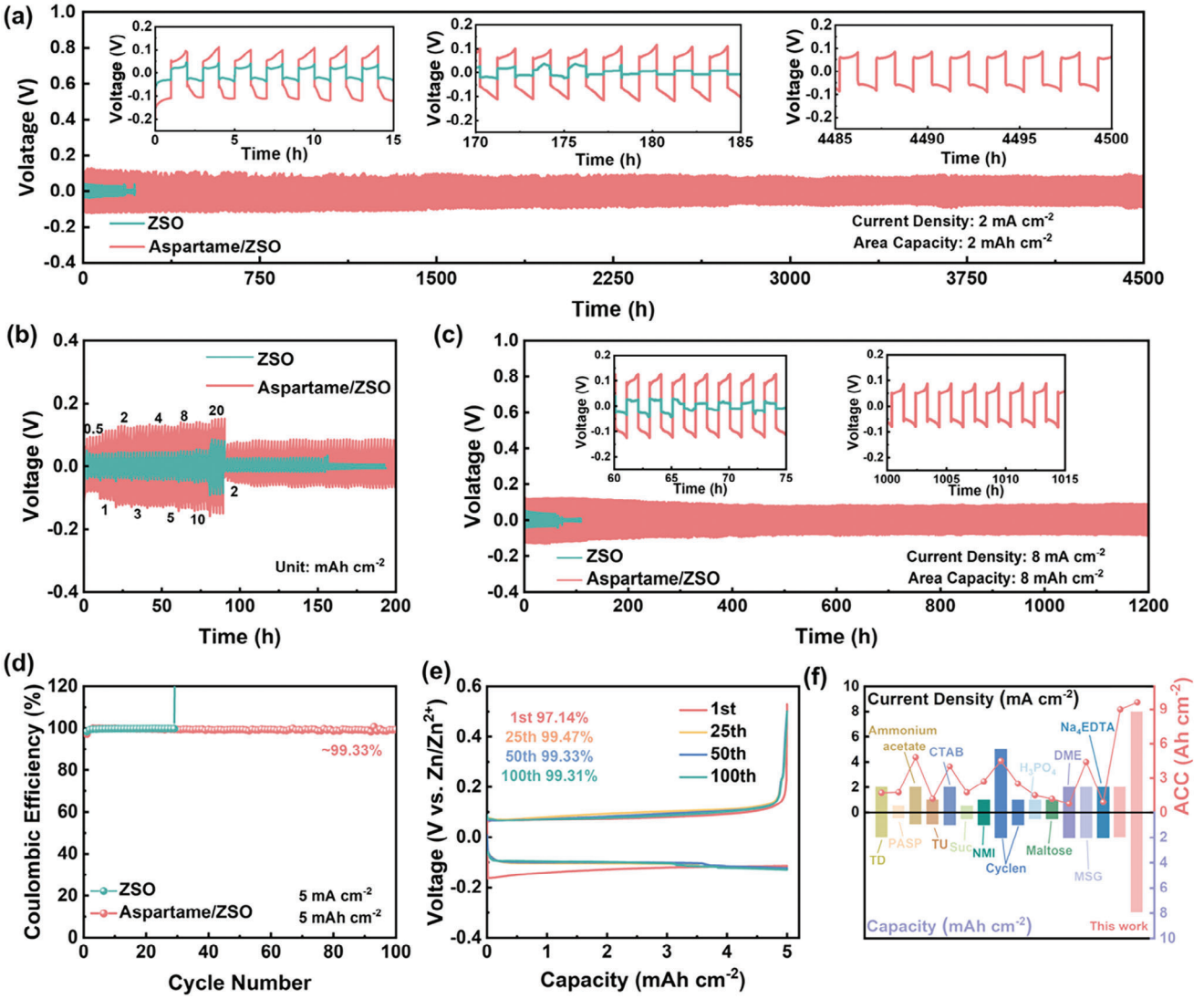

Figure 4. a) The voltage profile of Zn||Zn symmetric battery with different electrolytes cycling at 2 mA cm^{-2}, 2 mAh cm^{-2}, insets show magnified V–t curves. b) The rate performance of Zn||Zn cells. c) The voltage profile of Zn||Zn symmetric battery with different electrolytes cycling at 8 mA cm^{-2}, 8 mAh cm^{-2}. d) The CE curves of Zn||Cu half cells at 5 mA cm^{-2}, and e) corresponding voltage profiles. f) Comparison of cyclic stability of Zn||Zn cells among published reports of electrolytes modification strategy.

Cells with ZSO electrolyte failed within 80 cycles when the current density was set back to 2 mA cm^{-2}. Nevertheless, Aspartame/ZSO electrolytes showed stable operation under different current densities, and effective adaption to varying currents of up to 20 mA cm^{-2}. The extension of the lifespan of symmetric cells is also outstanding under other sets of current densities (90 h to more than 1200 h under 8 mA cm^{-2}, **Figure 5b**; 120 h to more than 1350 h under 5 mA cm^{-2}, Figure S16, Supporting Information) also substantiated that Aspartame is functional for improving stability under a wide range of current densities.

The reversibility was evaluated through measuring Coulombic Efficiency (CE) in Zn||Cu cells, and stability with limited zinc supply (70% and 80% depth of discharge). Under current density at 5 mA cm^{-2}, a superior CE of 99.33% can be reached after stably operating for 100 cycles, and CE up to 99.78% and 99.07% were realized at 8 and 2 mA cm^{-2}, respectively (Figure S17, Supporting Information), revealing perfect match between deposited zinc and copper substrate lattices, and outstanding utilization efficiency of zinc. These values are comparable with other reported work with electrolyte additives (Table S2, Supporting Information). On the contrary, CE rose suddenly at the 28th cycle followed by cell failure. This utilization rate of zinc is also supported by depth of discharge (DoD) tests. The zinc was first deposited on copper foil under 10 mA cm^{-2} for 1 h to prepare an electrode with 10 mAh zinc, then the Zn@Cu||Zn cell would cycle with a current density equal to 8 and 7 mA cm^{-2} representing 80% and 70% DoD correspondingly. As demonstrated in Figure S18 (Supporting Information), cells with ZSO electrolyte cycled stably for ≈25 h with both 70% and 80% DoD, and then a dramatic voltage increase happened demonstrating insufficient zinc supply due to poor reversibility. Nevertheless, Aspartame/ZSO

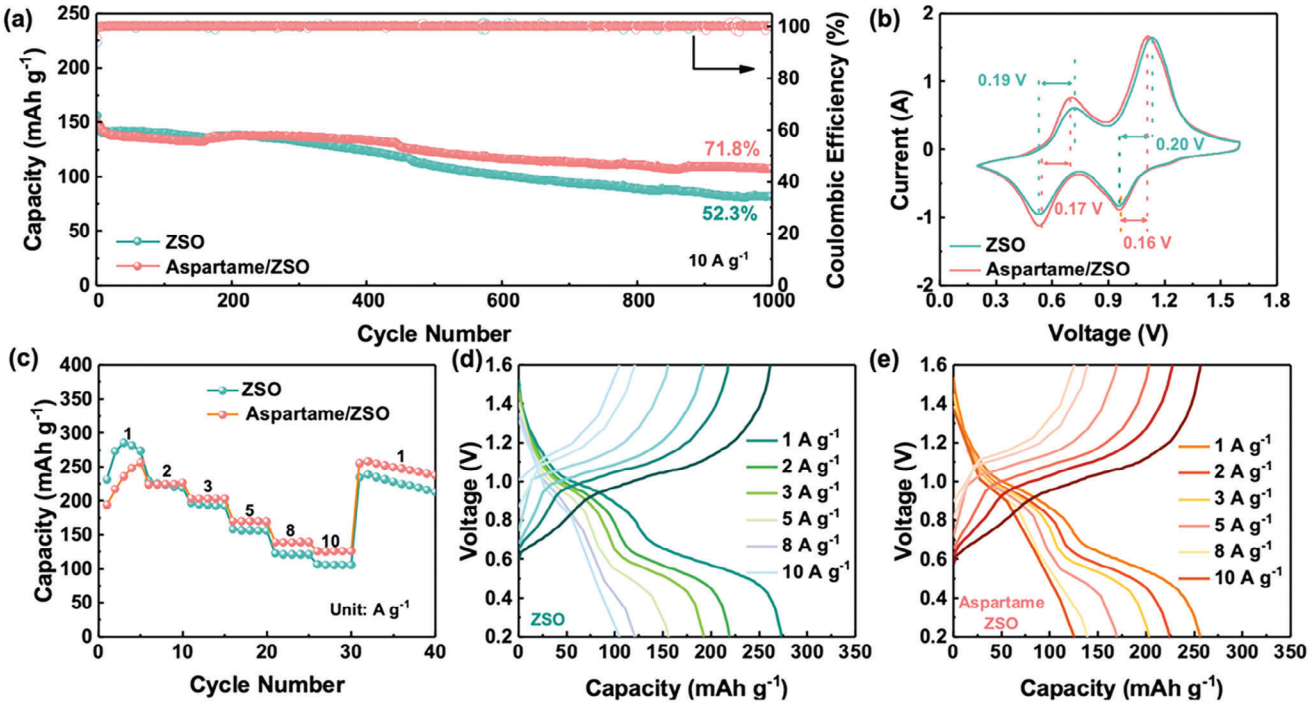

Figure 5. a) Cycling performance of Zn||$Cu_xV_2O_5$ cells at the current density of 10 A g^{-1}. b) CV curves of Zn||$Cu_xV_2O_5$ cells at a scan rate of 0.5 mV s^{-1}. c) The voltage profiles of Zn||$Cu_xV_2O_5$ cells showing the rate performance. Galvanostatic charge–discharge curves of Zn||$Cu_xV_2O_5$ batteries with d) ZSO and e) Aspartame/ZSO electrolyte at different current densities.

electrolyte could operate with 70% DoD stably for more than 300 h, and even with 80% DoD, stable operation would exceed 150 h.

Besides confirming improvement in zinc anode stability and reversibility, the practicable application of Aspartame/ZSO electrolyte was affirmed through Zn||$Cu_xV_2O_5$ cells. Through the hydrothermal method, Cu^{2+} and H_2O molecules were successfully co-inserted into V_2O_5 as demonstrated through XRD results (Figure S19, Supporting Information). The final $Cu_xV_2O_5{\cdot}nH_2O$ cathode was porous with a uniform distribution of Cu^{2+} as demonstrated through SEM and elemental mapping (Figure S20, Supporting Information). As indicated by the cyclic voltammetry (CV) profile scanned with the current rate of 0.5 mV s^{-1}, two pairs of typical index peaks representing the insertion and extraction of Zn^{2+} can be observed (Figure 5b). The comparison between CV profiles of ZSO and Aspartame/ZSO electrolytes showed similar locations of redox peaks, indicating no unpredictable side reactions. Moreover, the potential difference for two pairs of redox couples showed a decreasing trend, meaning lower overpotentials with the addition of Aspartame, and thereby the reversibility is improved. For evaluating rate performance with the addition of Aspartame, full cells were cycled with specific current densities from 1 to 10 A g^{-1} for 5 cycles under each current density, then continued to long-term cycling under 1 A g^{-1}. Because of higher nucleation potential and process of surface adsorption, full cells with Aspartame/ZSO require longer time for activation, so initial capacity under 1 A g^{-1} is lower than ZSO electrolyte. However, after stabilization and back to 1 A g^{-1}, Zn||$Cu_xV_2O_5$ full cells exhibited a high specific discharge capacity of 255.36 mAh g^{-1} with Aspartame/ZSO electrolyte (Figure 5c). Even at 10 A g^{-1}, the specific capacity can reach 125.8 mAh g^{-1}. Cycling stability under different current densities with modified electrolytes was also tested. As indicated by Figure 5a, when the specific current density is 10 A g^{-1}, the capacity after 1000 cycles remains 81.68 mAh g^{-1}, which is only 52.3% of the maximum capacity (Figure S21, Supporting Information). This poor capacity retention indicates unfavorable cycling stability. On the contrary, Aspartame helped improve the capacity retention up to 71.8% of the maximum capacity, which is 107.52 mAh g^{-1}. This improvement in capacity retention can also be observed under other specific current densities. At 5 A g^{-1}, capacity retention increases from 27.9% to 45.2% (Figure S22, Supporting Information). Overall, combined results illustrated multiple and outstanding advantages of Aspartame for zinc-metal-based energy storage and conversion systems. Moreover, taking the consideration of dissolution of $Cu_xV_2O_5$ issues, Zn||Polyaniline (Zn||PANi) full cells were also tested, and also showed favorable capacity retention (Figure S23, Supporting Information). Under 5 A g^{-1}, the capacity retention can reach 84.3% after 500 cycles, and under 10 A g^{-1}, the capacity retention can reach 83.0% after 900 cycles.

3. Conclusion

In summary, Methyl l-α-aspartyl-l-phenylalaninate (Aspartame) is applied as an effective electrolyte additive into the conventional 2.0 M $ZnSO_4$ electrolyte system to improve the stability of the zinc anode. Based on the theoretical calculation and series of spectroscopy techniques, Aspartame shows functions for modifying Zn^{2+} solvation structure and adhesion between the zinc surface. By substituting water molecules in the solvation

sheath, H_2O-induced parasitic reactions are dramatically suppressed, and adsorbed functional groups provide a driving force for uniform deposition. Combining all these merits, Zn||Zn symmetric cells with Aspartame/ZSO electrolyte reach an ultralong lifespan of more than 4500 h under 2 and 2 mAh cm^{-2}, showing surprising stability. The high reversibility and utilization efficiency of zinc were also confirmed through favorable stability with insufficient zinc supply and superior Coulombic Efficiency. Even at a high DoD of 70%, Zn||Zn symmetric cells still function stably for more than 300 h, and more encouragingly, Coulombic Efficiency can reach 99.33% under 5 mA cm^{-2}. This improvement in zinc anode also shows potential for zinc application by promoting capacity retention in full cells. Fabricated Zn||$Cu_xV_2O_5$ full cells can keep a capacity of 107.52 mAh g^{-1} after 1000 cycles under 10 A g^{-1}, corresponding to a capacity retention of 71.8%. Our findings proposed a novel additive for solving key issues in AZMBs with a trace amount of addition, paving the way for practicable application and further commercialization of aqueous Zn metal batteries for next-generation energy storage.

4. Experimental Section

Electrolyte Preparation: The 2.0 M $ZnSO_4$ electrolyte was prepared using $ZnSO_4{\cdot}7H_2O$ (Alfa Aesar), and deionized water in a flask. Electrolytes with additives were added Methyl l-α-aspartyl-l-phenylalaninate (Aspartame) (Macklin) with different concentrations (1.0, 5.0, 10.0, and 20.0 mM). To avoid errors caused by weighting trace amounts of additives, electrolytes with 1.0 mM Aspartame were prepared for 500 mL at once. The optimized electrolyte was 2.0 M $ZnSO_4$ with 10.0 mM Aspartame, which was denoted as Aspartame/ZSO electrolyte.

Preparation of $Cu_xV_2O_5{\cdot}nH_2O$ Cathode: The synthesis method of the Vanadium-based cathode was from ref. [4c]. Three hundred fifty-six milligrams of V_2O_5 (Macklin), 2 mL H_2O_2, and 75 mg $Cu(NO_3)_2$ (Macklin) were added into 60 mL deionized water in order. With the addition of H_2O_2 and $Cu(NO_3)_2$, the yellow turbid solution turned into a dark red solution. The solution was placed into a 100 mL Teflon-lined autoclave for hydrothermal treatment. After heating under 120 °C for 12 h, the final products were washed with water and ethanol. After being dried under 80 °C for 12 h, the brown powder was collected and defined as $Cu_xV_2O_5{\cdot}nH_2O$ because of the co-insertion of Cu^{2+} and H_2O. The $Cu_xV_2O_5{\cdot}nH_2O$ powder was mixed with Super P conductive carbon and polyvinylidene fluoride (PVDF) with a weight ratio of 7:2:1 in N-methyl-2-pyrrolidone (NMP) and meshed in the mortar to form a homogeneous slurry. The slurry was then coated on the stainless foil with the blade coating method and dried at 80 °C overnight.

More details about materials characterization, electrochemical characterization, simulation, and DFT calculation are provided in Supporting Information.

Supporting Information

Supporting Information is available from the Wiley Online Library or from the author.

Acknowledgements

M.T. and Q.L. contributed equally to this work. The work described in this paper was supported by a grant from Research Institute for Advanced Manufacturing at The Hong Kong Polytechnic University (CD8Z), and this work was also supported by the Hong Kong PhD Fellowship Scheme (PF21-65328).

Conflict of Interest

The authors declare no conflict of interest.

Data Availability Statement

The data that support the findings of this study are available from the corresponding author upon reasonable request.

Keywords

aspartame, solvation structure, surface adsorption, Zn metal batteries

Received: April 29, 2024
Revised: May 30, 2024
Published online: June 9, 2024

[1] X. Zou, M. Tang, Q. Lu, Y. Wang, Z. Shao, L. An, *Energy Environ. Sci.* **2024**, *17*, 386.
[2] J. Cao, D. Zhang, X. Zhang, Z. Zeng, J. Qin, Y. Huang, *Energy Environ. Sci.* **2022**, *15*, 499.
[3] Q. Lu, X. Zou, X. Wang, L. An, Z. Shao, Y. Bu, *Appl. Catal., B* **2023**, *325*, 122323.
[4] a) Q. Cao, Y. Gao, J. Pu, X. Zhao, Y. Wang, J. Chen, C. Guan, *Nat. Commun.* **2023**, *14*, 641; b) Y. Du, X. Chi, J. Huang, Q. Qiu, Y. Liu, *J. Power Sources* **2020**, *479*, 228808; c) Q. Liu, Z. Yu, R. Zhou, B. Zhang, *Adv. Funct. Mater.* **2022**, *33*, 2210290; d) C. Xie, S. Liu, Z. Yang, H. Ji, S. Zhou, H. Wu, C. Hu, Y. Tang, X. Ji, Q. Zhang, H. Wang, *Angew. Chem., Int. Ed.* **2023**, *62*, 202218612.
[5] a) Y. Hao, J. Zhou, G. Wei, A. Liu, Y. Zhang, Y. Mei, B. Lu, M. Luo, M. Xie, *ACS Appl. Energy Mater.* **2021**, *4*, 6364; b) T. Li, S. Hu, C. Wang, D. Wang, M. Xu, C. Chang, X. Xu, C. Han, *Angew. Chem., Int. Ed.* **2023**, *62*, 202314883; c) J. Yang, R. Zhao, Y. Wang, Y. Bai, C. Wu, *Energy Mater. Adv.* **2022**, *2022*, 1; d) J. Yang, R. Zhao, Y. Wang, Z. Hu, Y. Wang, A. Zhang, C. Wu, Y. Bai, *Adv. Funct. Mater.* **2023**, *33*, 2213510.
[6] a) Y. Geng, L. Pan, Z. Peng, Z. Sun, H. Lin, C. Mao, L. Wang, L. Dai, H. Liu, K. Pan, X. Wu, Q. Zhang, Z. He, *Energy Storage Mater.* **2022**, *51*, 733; b) X. Gong, H. Yang, J. Wang, G. Wang, J. Tian, *ACS Appl. Mater. Interfaces* **2023**, *15*, 4152; c) Z. Liu, R. Wang, Y. Gao, S. Zhang, J. Wan, J. Mao, L. Zhang, H. Li, J. Hao, G. Li, L. Zhang, C. Zhang, *Adv. Funct. Mater.* **2023**, *33*, 2308463.
[7] a) L. Wang, W. Huang, W. Guo, Z. H. Guo, C. Chang, L. Gao, X. Pu, *Adv. Funct. Mater.* **2021**, *32*, 2108533; b) Q. Zhang, J. Luan, X. Huang, Q. Wang, D. Sun, Y. Tang, X. Ji, H. Wang, *Nat. Commun.* **2020**, *11*, 3961.
[8] a) J. Jiang, Z. Pan, J. Yuan, J. Shan, C. Chen, S. Li, HaiXu, Y. C., Q. Zhuang, Z. Ju, H. Dou, X. Zhang, J. Wang, *Chem. Eng. J.* **2023**, *452*, 139335; b) X. Zou, Q. Lu, C. Wang, S. She, K. Liao, R. Ran, W. Zhou, L. An, Z. Shao, *J. Membr. Sci.* **2023**, *665*, 121112.
[9] a) Y. Mu, Z. Li, B. K. Wu, H. Huang, F. Wu, Y. Chu, L. Zou, M. Yang, J. He, L. Ye, M. Han, T. Zhao, L. Zeng, *Nat. Commun.* **2023**, *14*, 4205; b) X. Zhang, Q. Ruan, L. Liu, D. Li, Y. Xu, Y. Wang, J. Liu, C. Huang, F. Xiong, B. Wang, P. K. Chu, *J. Electroanal. Chem.* **2023**, *936*, 117357.
[10] a) Z. Li, Y. Liao, Y. Wang, J. Cong, H. Ji, Z. Huang, Y. Huang, *Energy Storage Mater.* **2023**, *56*, 174; b) F. Ming, Y. Zhu, G. Huang, A. H. Emwas, H. Liang, Y. Cui, H. N. Alshareef, *J. Am. Chem. Soc.* **2022**, *144*, 7160.
[11] J. H. Chong Zhang, X. Wu, A. Daniyar, L. Zhu, C. Chen, D. P. Leonard, I. A. Rodríguez-Pérez, J.-X. Jiang, C. Fang, X. Ji, *Chem. Commun.* **2018**, *54*, 14097.
[12] D. E. Ciurduc, C. d. l. Cruz, N. Patil, A. Mavrandonakis, R. Marcilla, *Energy Storage Mater.* **2022**, *53*, 532.

[13] M. Luo, C. Wang, H. Lu, Y. Lu, B. B. Xu, W. Sun, H. Pan, M. Yan, Y. Jiang, *Energy Storage Mater.* **2021**, *41*, 515.
[14] N. Wang, S. Zhai, Y. Ma, X. Tan, K. Jiang, W. Zhong, W. Zhang, N. Chen, W. Chen, S. Li, G. Han, Z. Li, *Energy Storage Mater.* **2021**, *43*, 585.
[15] P. Sun, L. Ma, W. Zhou, M. Qiu, Z. Wang, D. Chao, W. Mai, *Angew. Chem., Int. Ed.* **2021**, *60*, 18247.
[16] K. Zhao, G. Fan, J. Liu, F. Liu, J. Li, X. Zhou, Y. Ni, M. Yu, Y. M. Zhang, H. Su, Q. Liu, F. Cheng, *J. Am. Chem. Soc.* **2022**, *144*, 11129.
[17] M. Li, S. Luo, Y. Qian, W. Zhang, L. Jiang, J. Shen, *J. Electrochem. Soc.* **2007**, *154*, D567.
[18] A. Bani Hashemi, G. Kasiri, F. La Mantia, *Electrochim. Acta* **2017**, *258*, 703.
[19] S. J. Zhang, J. Hao, D. Luo, P. F. Zhang, B. Zhang, K. Davey, Z. Lin, S. Z. Qiao, *Adv. Energy Mater.* **2021**, *11*, 2102010.
[20] A. Bayaguud, X. Luo, Y. Fu, C. Zhu, *ACS Energy Lett.* **2020**, *5*, 3012.
[21] J. Zhao, J. Zhang, W. Yang, B. Chen, Z. Zhao, H. Qiu, S. Dong, X. Zhou, G. Cui, L. Chen, *Nano Energy* **2019**, *57*, 625.
[22] W. Yang, X. Du, J. Zhao, Z. Chen, J. Li, J. Xie, Y. Zhang, Z. Cui, Q. Kong, Z. Zhao, C. Wang, Q. Zhang, G. Cui, *Joule* **2020**, *4*, 1557.
[23] D. Wang, Q. Li, Y. Zhao, H. Hong, H. Li, Z. Huang, G. Liang, Q. Yang, C. Zhi, *Adv. Energy Mater.* **2022**, *12*, 2102707.
[24] H. Yu, D. Chen, T. Zhang, M. Fu, J. Cai, W. Wei, X. Ji, Y. Chen, L. Chen, *Small Struct.* **2022**, *3*, 2200143.
[25] W. Zhang, Y. Chen, H. Gao, W. Xie, P. Gao, C. Zheng, P. Xiao, *Mater. Futures* **2023**, *2*, 042102.
[26] T. C. Li, Y. Lim, X. L. Li, S. Luo, C. Lin, D. Fang, S. Xia, Y. Wang, H. Y. Yang, *Adv. Energy Mater.* **2022**, *12*, 2103231.
[27] H. Yang, Z. Chang, Y. Qiao, H. Deng, X. Mu, P. He, H. Zhou, *Angew. Chem., Int. Ed.* **2020**, *59*, 9377.
[28] Z. Cheng, K. Wang, J. Fu, F. Mo, P. Lu, J. Gao, D. Ho, B. Li, H. Hu, *Adv. Energy Mater.* **2024**, *14*, 2304003.
[29] Z. Hou, Y. Gao, R. Zhou, B. Zhang, *Adv. Funct. Mater.* **2021**, *32*, 2107584.